Higgs dynamics in the early universe

Vis, J.M. van de

Part I

Reheating the universe after inflation

Chapter 2

Introduction to reheating

Immediately after the end of inflation, the dominant constituent of the universe is the inflaton field that is oscillating at the bottom of its potential. The densities of all other particles have been diluted to practically zero during inflation. We have seen in the introduction that inflation should connect to standard HBB cosmology. The energy of the inflaton field must be transferred to the SM degrees of freedom. The successful predictions of BBN give a lower bound on the energy scale at which this transition needs to be complete. To explain BBN, the universe needs to be radiation-dominated and the SM particles in chemical equilibrium at $T_{\rm BBN}$. We therefore know that the transfer of energy from the inflaton field to the SM particles, as well as their thermalization, must have completed before the era of Big Bang Nucleosynthesis.

The process of energy transfer from the inflationary sector to the standard model particles and the subsequent thermalization, is referred to as reheating. In early studies of reheating it was assumed that the inflaton decays into SM particles through perturbative interactions [79–81]. It was realized in Refs. [82–89] that the coherent oscillations of the inflaton field can lead to a phase of resonant particle production. This phase is referred to as the preheating stage. For some inflationary models, preheating is so efficient that the inflaton field can transfer all of its energy during this stage. In other cases some early resonant energy transfer takes place, but perturbative decays are needed for reheating to complete.

In this introductory chapter we will first motivate why the reheating phase is interesting to study. We will then lay out some basics of particle production.

2.1 Why is studying reheating important?

Even though the reheating phase can not be probed directly, it is an interesting phase to study, for a variety of reasons.

2.1.1 Reheating temperature

The end state of reheating is a universe filled with SM particles in equilibrium (as we will see below, DM might be produced during reheating as well). Typically, the reheating temperature, $T_{\rm reh}$, is estimated from the energy density at the end of reheating, $\rho_{\rm reh}$, through the relation

$$\rho_{\rm reh} = \frac{\pi^2}{30} g_*(T_{\rm reh}) T_{\rm reh}^4 \,, \tag{2.1}$$

where $g_*(T_{\rm reh})$ is the number of relativistic degrees of freedom at the reheating temperature.

As mentioned above, the value of the reheating temperature is constrained by the predictions of Big Bang Nucleosynthesis (see section 1.2.2.3). Taking the temperature at which BBN took place as a lower bound on the reheating temperature gives $T_{\rm reh} > T_{\rm BBN} \approx 1\,\text{MeV}$. When the effect of the relic neutrino background on the abundances of light elements is taken into account, the constraint becomes slightly stronger: $T_{\rm reh} \gtrsim 4\,\text{MeV}$ [90, 91].

2.1.2 Expansion rate after inflation

In section 1.2.1 we introduced the equation of state parameter w

$$w = \frac{P}{\rho} \,, \tag{2.2}$$

which determines the time-dependence of the scale factor and the dependence on the scale factor of the energy density.

Since the Hubble parameter is defined as the logarithmic derivative of the scale factor, the above relation determines how the comoving size of the horizon or inverse Hubble scale $(aH)^{-1}$ depends on the scale factor a. The (smallest) momentum scale k of the modes of the fluctuations in the CMB that are observed today is given by the current value of the Hubble scale: $k = a_0 H_0$. The amplitude of this mode was set when it became superhorizon during inflation, which happened when the momentum was equal to the Hubble scale during inflation: $k = aH$.

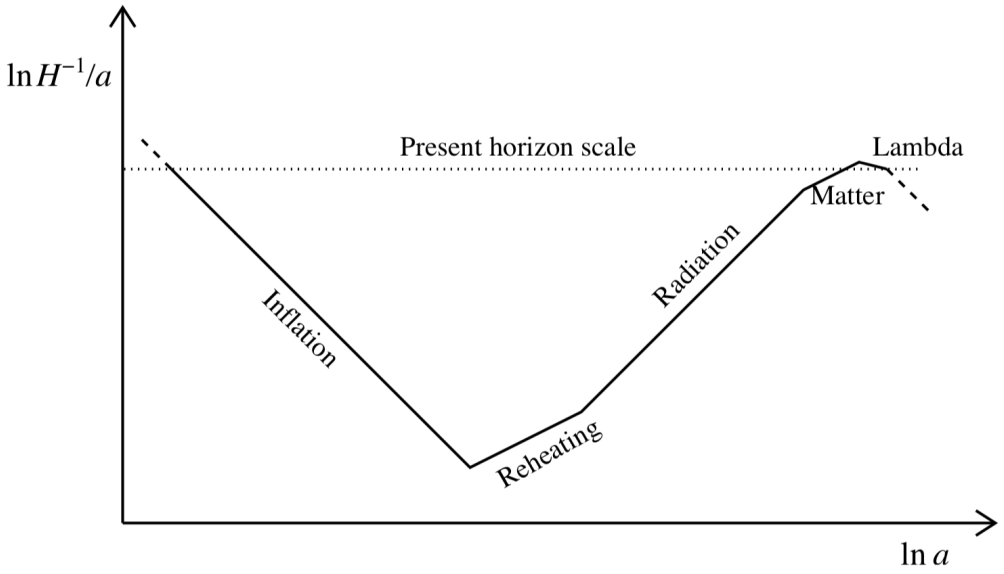

FIGURE 2.1: The logarithm of the Hubble scale as a function of the scale factor during and after inflation, illustrating how the dependence of the Hubble scale on the scale factor varies for the different epochs. The dashed lines show extrapolations to the past and future. Figure copied from Ref. [92].

For a given model of inflation, the local properties of the potential can be determined from observations of the CMB. In order to use CMB-observables to constrain inflationary models, one must know at what moment during inflation the perturbations that are observed today were formed. This moment determines the value of the inflationary potential, which in turn gives the values of the observable primordial tilt and tensor-to-scalar ratio. To find this moment during inflation, the expansion history after inflation should be known. Knowing the equation of state *after* inflation tells us how many e-folds passed since the end of inflation until now. This determines the amount of e-folds between the generation of the perturbation at $k = aH$ and the end of inflation, as is clearly explained in Refs. [92, 93]. This is illustrated in figure 2.1, that shows the expansion history during the different epochs (with different equations of state) that the universe went through.

The equation of state during reheating depends on the shape of the inflationary potential. For example, an inflaton oscillating in a quadratic potential gives rise to a matter-like equation of state $w = 0$ and an inflaton oscillating in a quartic potential to a radiation-like equation of state $w = 1/3$. When reheating completes and the universe becomes radiation-dominated, the equation of state relaxes to $w = 1/3$. The expansion history is thus affected by the shape of the potential and the duration of reheating.

Figure 2.2 shows how the uncertainty in the expansion history after inflation affects the comparison of different inflationary models to CMB-observables. The small dots show the predictions for the

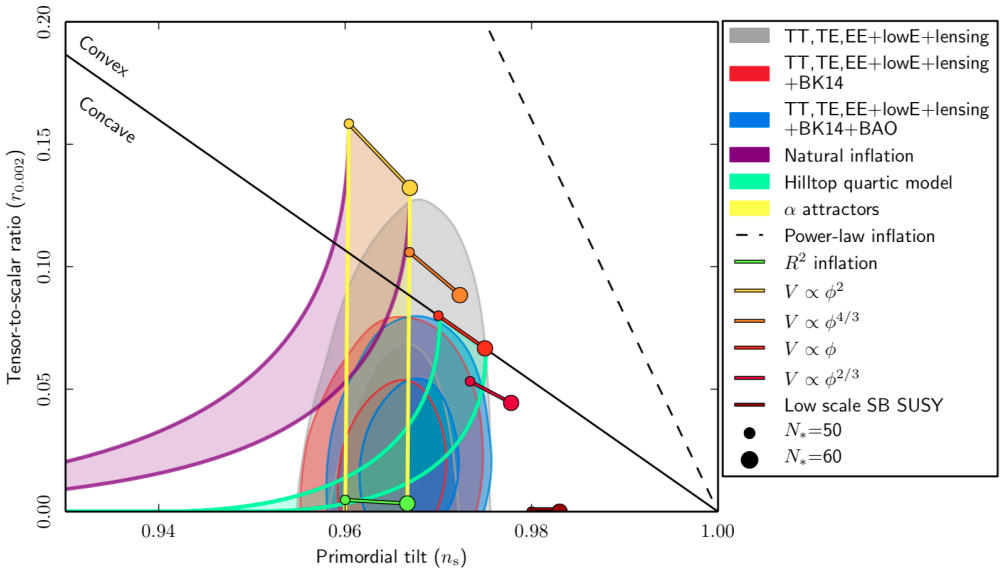

FIGURE 2.2: 68% and 95% confidence level regions for the primordial tilt n_s and tensor-to-scalar ratio r at $k = 0.002\,\mathrm{Mpc}^{-1}$ from *Planck* 2018 data alone (gray regions) and in combination with BICEP2/Keck Array 2014 data (red regions) and BICEP2/Keck Array 2014 and Baryon Acoustic Oscillation data (blue regions). The confidence intervals are compared with predictions for n_s and r for different inflationary models. Figure copied from Ref. [77].

primordial tilt n_s and tensor-to-scalar ratio r for the cases when the CMB-modes were formed 50 e-folds before the end of inflation and the large dot shows the prediction if the perturbations were formed 60 e-folds before the end of inflation. A better understanding of reheating would decrease the uncertainty in the evolution after inflation and would therefore shrink the uncertainty in comparisons like figure 2.2.

2.1.3 Higgs vacuum stability

The possible decay of the electroweak vacuum during preheating is the topic of chapter 3. In this chapter, we consider a Higgs potential with a quartic coupling that runs negative at large energy scales. This implies that the electroweak vacuum that we live in today is not the energetically favorable vacuum, but that there is a state of even lower energy, the 'true vacuum' [94–100]. Decay to this true vacuum state would lead to rapidly growing bubbles with negative cosmological constant [101–105], that would take over the entire universe, which is clearly inconsistent with the universe that we live in. We study the production of Higgs quanta during reheating – in a model where the Higgs is not the inflaton – to determine whether in that model the Higgs field decays to the true vacuum state or not. Determining whether the Higgs vacuum remains stable during reheating can be a consistency check for models of inflation and BSM physics.

2.1.4 Generation of the baryon asymmetry

There are mechanisms for generating the baryon asymmetry of the universe during reheating. One example is the class of Grand Unified Theories (GUTs), in which the $SU(3)_C \times SU(2)_L \times U(1)_Y$-symmetry group of the SM is part of a larger symmetry group above the GUT energy scale. Above this scale, quarks and leptons are part of the same multiplets, and therefore baryon number B is not a conserved quantity, which allows for the generation of baryon number. Violation of B implies that the proton is not absolutely stable. Experiments aiming to observe proton decay so far have only put lower bounds on the lifetime of the proton, which severely constrains the simplest GUT, where the SM gauge group is a subgroup of $SU(5)$ [106]. In fact, non-supersymmetric $SU(5)$ is completely ruled out by the non-detection of proton decay [107]. Other symmetry groups that are still allowed by experiment and that can also break into the SM are for example $SO(10)$ (which also contains right-handed neutrinos), E_6, E_7 and E_8. Baryogenesis in GUTs can be realized when a heavy boson X is produced nonperturbatively during the preheating phase. The baryon asymmetry is generated when the unstable particle X decays into SM particles [108, 109].

Another possibility for generating the baryon asymmetry during preheating is the Cold Electroweak Baryogenesis model [110, 111]. Here, inflation happens at the electroweak scale (which is orders of magnitude lower than the inflationary scale in most other models). B-violating electroweak sphaleron transitions are active during preheating and the baryon asymmetry is formed. When reheating ends, the temperature of the universe is so low that B-violating processes have become inefficient, such that the generated baryon asymmetry remains.

In this part of the thesis we will not consider the possibility of generating the baryon asymmetry during reheating. Part II of this thesis treats the generation of the baryon asymmetry during the electroweak phase transition, assuming that reheating has already completed.

2.1.5 Dark matter production

It should not come as a surprise that the dark matter abundance can also be generated during the reheating phase. Two examples of dark matter candidates that can be produced during reheating:

- WIMPzillas [112, 113] are very heavy ($10^{12} - 10^{16}\,\mathrm{GeV}$) nonthermal dark matter candidates that are very long-lived. At the end of inflation, these particles can be produced gravitationally or through a direct coupling to the inflaton field. Decay of WIMPzilla particles could produce cosmic rays with ultra-high energies [114].

- Scalar fields that are non-minimally coupled to gravity can be produced during reheating through tachyonic resonance [115] (see also section 2.2.3.3). If the couplings of these scalars to the SM are small, they are long lived, and can form all of the observed dark matter (and escape all direct, indirect and collider searches [116]).

2.2 Particle production during reheating

In this section we will lay out the behavior of the inflaton field after inflation and the possible particle production mechanisms. Even though the equations governing the behavior of the inflaton field and the produced particles will mostly be solved numerically in the upcoming chapters, some intuition can be gained from analytic estimates. We will present these analytical estimates for single-field inflation in the upcoming part, following the analyses of Refs. [89, 117]. Other useful reviews of particle production after inflation are Refs. [118, 119].

2.2.1 Oscillating inflaton field

The equation of motion of the inflaton field is given by:

$$\ddot{\chi} + 3H\dot{\chi} + V_{,\chi} = 0\,, \tag{2.3}$$

where χ denotes the classical background value of the inflaton and the subscript $,\chi$ a derivative with respect to the field χ. The behavior of the inflaton field depends on the details of the potential. For concreteness, we will consider a quadratic potential

$$V(\chi) = \frac{1}{2}m^2\chi^2\,, \tag{2.4}$$

which is a good approximation for many inflationary models during reheating. At the end of inflation the field oscillates with decreasing amplitude. The evolution of the inflaton field asymptotes to

$$\chi(t) = X(t)\sin(mt)\,, \qquad X(t) \propto \frac{1}{mt}\,, \tag{2.5}$$

as is shown in figure 2.3.

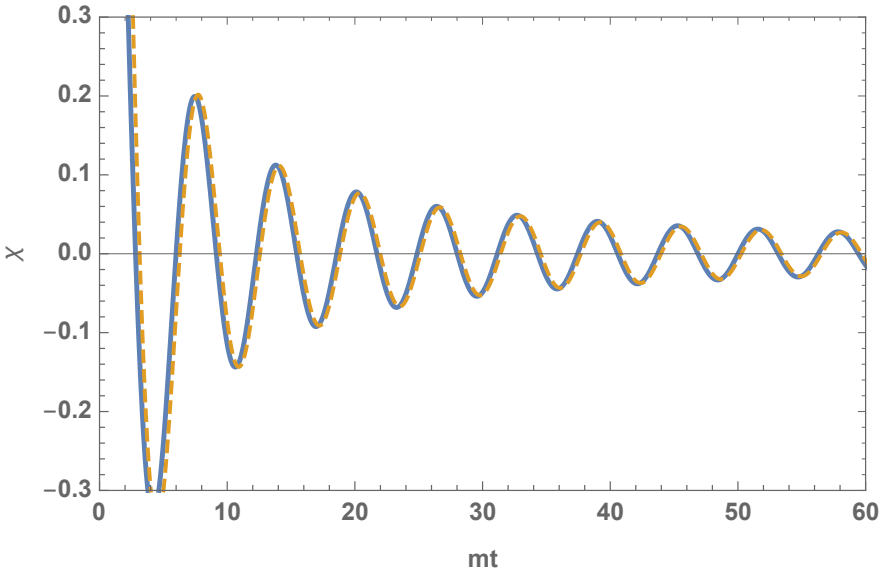

FIGURE 2.3: Numerical solution to eq. (2.3) for a quadratic potential with $m = 10^{-5} m_{\rm pl}$ (solid blue). The approximation of eq. (2.5) is shown in dashed orange.

2.2.2 Perturbative inflaton decay

Initially, particle production after inflation was described by perturbative decays of the inflaton field [80, 81]. As an example we consider an inflaton field that is coupled to a scalar field η and a spinor field ψ, with interaction term:

$$\mathcal{L}_{\rm int} = -\sigma\chi\eta^2 - h\chi\bar{\psi}\psi, \tag{2.6}$$

where σ is a mass scale and h is a dimensionless coupling. The $\sigma\chi\eta^2$-term for example arises from spontaneous symmetry breaking. Provided that the mass of the inflaton is larger than twice the mass of its decay product, the inflaton can decay into pairs of η- and ψ-particles, with the following decay rates [120]

$$\Gamma_{\chi\to\eta\eta} = \frac{\sigma^2}{8\pi m}\,, \qquad \Gamma_{\chi\to\bar{\psi}\psi} = \frac{h^2 m}{8\pi}\,. \tag{2.7}$$

Perturbative decay will only become efficient once the decay rates become comparable to the Hubble expansion rate

$$\Gamma_{\rm tot} \gtrsim H\,, \tag{2.8}$$

where $\Gamma_{\rm tot}$ is the sum of the perturbative decay rates. For realistic values of the couplings and masses, $\Gamma_{\rm tot} \ll H$ at the onset of reheating. As the universe expands, H decreases until it becomes equal to the decay rate. Using $H^2 = \frac{\rho}{3m_{\rm pl}^2}$ and eq. (2.1) gives the reheating temperature:

$$T_{\rm reh} \approx \left(\frac{90}{g_*\pi^2}\sqrt{m_{\rm pl}\Gamma_{\rm tot}}\right)\,. \tag{2.9}$$

The perturbative approach does not give a complete description of the reheating process. As we will see below, resonant particle production can be much more efficient than perturbative decays. In some cases, this so-called preheating phase is so efficient that the inflaton field rapidly transfers all of its energy before the resonance shuts off. Alternatively, the inflaton looses some of its energy during the preheating phase, but remains the dominant contribution to the energy budget of the universe when the resonance shuts off. In this case, reheating completes much later, through the perturbative decay described above.

2.2.3 Resonant particle production

The first reason why particle production can be much more efficient than the perturbative production, is that the decay of the inflaton field is a collective process – the inflaton quanta do not decay independently of each other. The second reason is that Bose condensation effects in the decay products can strongly enhance the production (this effect is not present for fermions). These effects are relevant for the initial phase of reheating, preheating. This phase should thus be studied in a non-perturbative analysis.

Let's consider production of the field η with mass m_η and coupling to the inflaton as in eq. (2.6). We first consider the regime $m_\eta > \sqrt{2\sigma X}$ [1]. In order to make analytic progress, we neglect the expansion of space, i.e. we take a=1. The mode equation of the η-field is given by

$$\ddot{\eta}_k + \left[k^2 + m_\eta^2 + 2\sigma X \sin(mt)\right] \eta_k \equiv \ddot{\eta}_k + \omega_k^2(t)\eta_k = 0\,. \tag{2.10}$$

The number density per k-mode is

$$n_k = \frac{\omega_k}{2}\left(\frac{|\dot{\eta}_k|^2}{\omega_k^2} + |\eta_k|^2\right) - \frac{1}{2}\,, \tag{2.11}$$

and the full number density n_η and energy density ρ_η can be obtained by integrating over all k-modes:

$$n_\eta = \frac{1}{2\pi^2}\int_0^\infty dk k^2 n_k\,, \qquad \rho_\eta = \frac{1}{2\pi^2}\int_0^\infty dk k^2 \omega_k n_k\,. \tag{2.12}$$

[1] If we allow $m_\eta < \sqrt{2\sigma X}$, for small k-modes the effective η-mass squared becomes negative during part of the oscillation. This is the tachyonic resonance regime that is described in section 2.2.3.3

In order to solve eq. (2.10), we make a change of variables and rewrite eq. (2.10) in the form of a Mathieu equation [121, 122]

$$\begin{aligned} &\eta_k'' + [A_k - 2q\cos 2z]\,\eta_k = 0\,, \\ &A_k = 4\frac{k^2 + m_\eta^2}{m^2}\,, \quad q = \frac{4\sigma X}{m^2}\,, \quad z = \frac{mt}{2}\,, \end{aligned} \tag{2.13}$$

where a prime denotes derivative with respect to z. The solutions to the Mathieu equation can be described by the stability and instability bands of figure 2.4. Modes with values of A_k and q lying in an instability band display exponential growth:

$$\eta_k \propto \exp\left[\mu_k z\right]\,. \tag{2.14}$$

As becomes clear from figure 2.4, the range of k-modes that gets resonantly enhanced depends on q. For small values of $q \ll 1$ only a small range of k-modes gets resonantly produced. This regime is called narrow resonance. For larger values of $q > 1$, a wider range of k-modes gets enhanced – this is called the broad resonance regime. Both cases are described below.

2.2.3.1 Narrow resonance

Narrow resonance occurs when $q \ll 1$. Only k-modes for which $A_k \approx n^2$, with n an integer, get enhanced. The first resonant band at $A_k \approx 1$ is the most important one and occurs for momenta in the range $k = \frac{m}{2}\left(1 \pm \frac{q}{2}\right)$. The rate of exponential growth for k-modes in the first instability band is given by

$$\mu_k = \sqrt{\left(\frac{q}{2}\right)^2 - \left(\frac{2k}{m} - 1\right)^2}\,. \tag{2.15}$$

The growth of the particle number density in the fastest growing mode is shown in the left panel of figure 2.5.

The well-understood picture of narrow resonance in Minkowski space does not completely carry over to an expanding universe. Due to gravitational redshift, k-modes might not remain in the instability bands for a long enough time to get exponentially enhanced. This leads to the additional requirement for resonant production:

$$q^2 m \gtrsim H\,, \tag{2.16}$$

which is typically not satisfied at the end of inflation for $q \ll 1$, such that the narrow resonance does not take off. At a later stage of reheating narrow resonance can nevertheless become important [84].

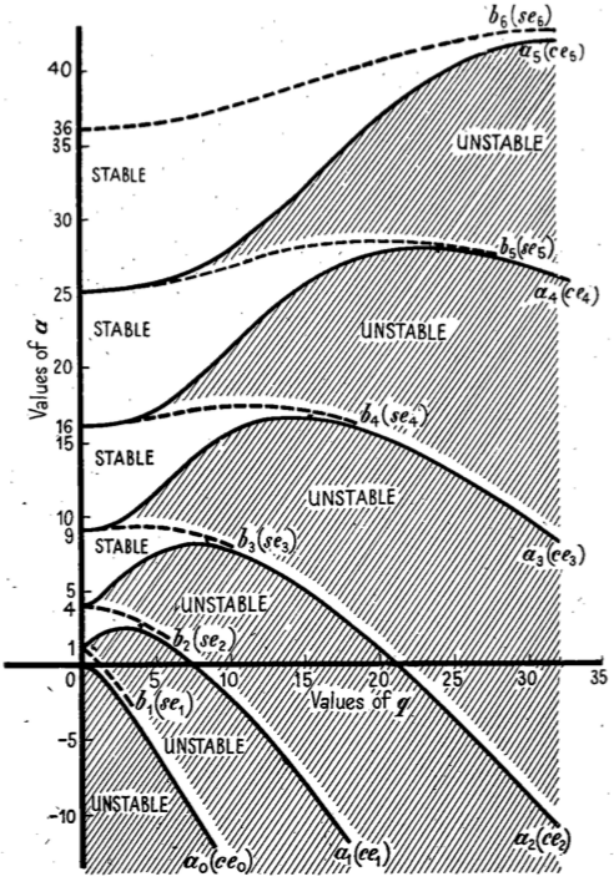

FIGURE 2.4: Stability and instability bands of the Mathieu equation (2.13). The horizontal axis shows the value of q and the vertical axis shows the value of A_k. The white regions correspond to stable solutions while the shaded areas correspond to exponentially growing solutions. Figure copied from Ref. [121].

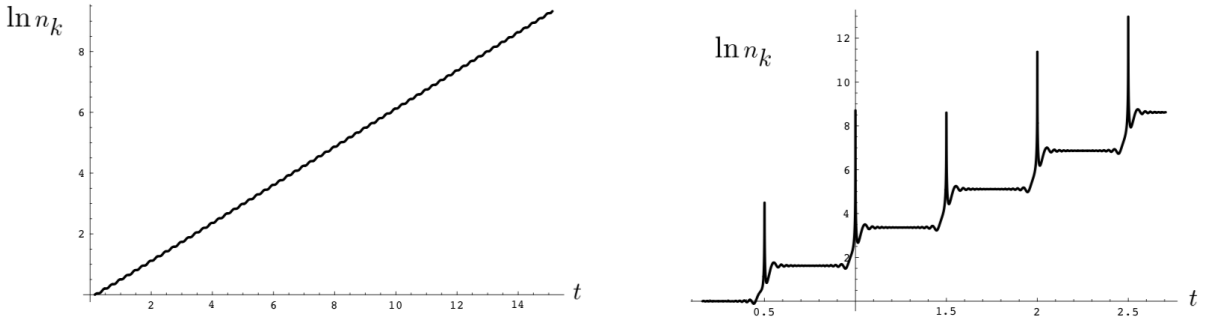

FIGURE 2.5: Number density in the fastest growing k-mode as a function of time during parametric resonance. The left panel shows narrow resonance for $q \approx 0.1$ and the right panel shows broad resonance for the potential of eq. (2.4). In both cases the expansion of spacetime is neglected. Time is shown in units of $\frac{m}{2\pi}$. Figure copied from Ref. [89].

2.2.3.2 Broad resonance

It is clear from figure 2.4 that the gray instability bands become wider for $q > 1$. This is therefore called the broad resonance regime. In this regime, particle production is typically very efficient. Modes with momentum k get resonantly produced when the adiabaticity condition

$$\frac{d\omega_k}{dt} \gtrsim \omega_k^2 \,, \tag{2.17}$$

is violated. In our toy model, these bursts of particle production happen when the (inflaton-dependent) mass of the decay product becomes very small, as the inflaton field crosses zero. In chapter 4 we will see an example of particle production where the violation of adiabaticity is not caused by a small mass, but by the derivative of the mass becoming large. The right panel of figure 2.5 shows the time dependence of the particle number density in the broad resonance regime. In contrast to the narrow resonance case, particles are only produced when $\chi(t) \approx 0$ and the number density remains approximately constant between two subsequent bursts. An analytic treatment of broad resonance in a static spacetime can be found in Refs. [89, 117].

Again, taking the expansion of the universe into account, the picture changes. Since the amplitude of the inflaton field now decreases with time, q decreases and the resonance becomes more narrow. Explosive particle production can however still occur. The theory of broad resonance in an expanding universe is called 'stochastic resonance'. We will not pursue it any further in this introduction, since we will solve our mode equations numerically in the upcoming chapters.

2.2.3.3 Tachyonic resonance

The narrow and broad resonance cases described above correspond to the regime $A_k \leq 2q$. In this regime ω_k^2 is always positive and (in the broad resonance case) particle production occurs when eq. (2.17) is satisfied. If we drop the condition that $m_\eta > \sqrt{2\sigma X}$, k-modes with

$$k^2 < 2\sigma X - m_\eta^2 \,, \tag{2.18}$$

have $\omega_k^2 < 0$ during part of the oscillation. The 'tachyonic resonance' that occurs during this period can be extremely efficient [123–126]. An extensive analytical and numerical study of tachyonic preheating is given in Ref. [124]. Tachyonic resonance can occur in theories with trilinear couplings,

like our example eq. (2.6), but also for fields coupling to the spacetime Ricci tensor R, as we will see in chapter 3.